NESSI: the New Mexico Tech Extrasolar Spectroscopic Survey Instrument

C. Jurgenson*[a], F. Santoro[a], M. Creech-Eakman[a], K. Houairi[a], H. Bloemhard[a], G. Vasisht[b], M. Swain[b], P. Deroo[b], C. Moore[b], L. Schmidt[a], P. Boston[a], D. Rodeheffer[a], P. Chen[b]

[a]New Mexico Tech, 801 Leroy Place, Socorro, NM, USA 87801;
[b]Jet Propulsion Lab, 4800 Oak Grove Drive, Pasadena, CA USA 00555-9642

ABSTRACT

Less than 20 years after the discovery of the first extrasolar planet, exoplanetology is rapidly growing with more than one discovery every week on average since 2007. An important step in exoplanetology is the chemical characterization of exoplanet atmospheres. It has recently been shown that molecular signatures of transiting exoplanets can be studied from the ground. To advance this idea and prepare more ambitious missions such as THESIS, a dedicated spectrometer named the New Mexico Tech Extrasolar Spectroscopic Survey Instrument (NESSI) is being built at New Mexico Tech in collaboration with the NASA Jet Propulsion Laboratory. NESSI is a purpose-built multi-object spectrograph that operates in the J, H, and K-bands with a resolution of R = 1000 in each, as well as a lower resolution of R = 250 across the entire J/H/K region.

Keywords: MRO, exoplanet atmosphere, multi-object spectrograph, near infrared

1. INTRODUCTION

Since 1992, when the first exoplanets around the pulsar PSR B1257+12 were discovered, the study of exoplanets has become a diverse and fast-moving field[1]. As of July 2010, there are 464 known exoplanets[2]. The vast majority of exoplanets were discovered using radial velocity measurements, which allows several orbital parameters and the minimum mass of the exoplanet to be determined. Using the transit method, we can further restrict the mass of the exoplanet as well as determine its radius and probe its atmosphere. The transit method is only useful in systems in which the exoplanet passes directly in front of the parent star. There are more than 80 such systems that have been confirmed[2]. Transiting exoplanets are the only ones for which we have the potential to learn the physical structure in enough detail to make direct comparisons with the planets of our solar system.
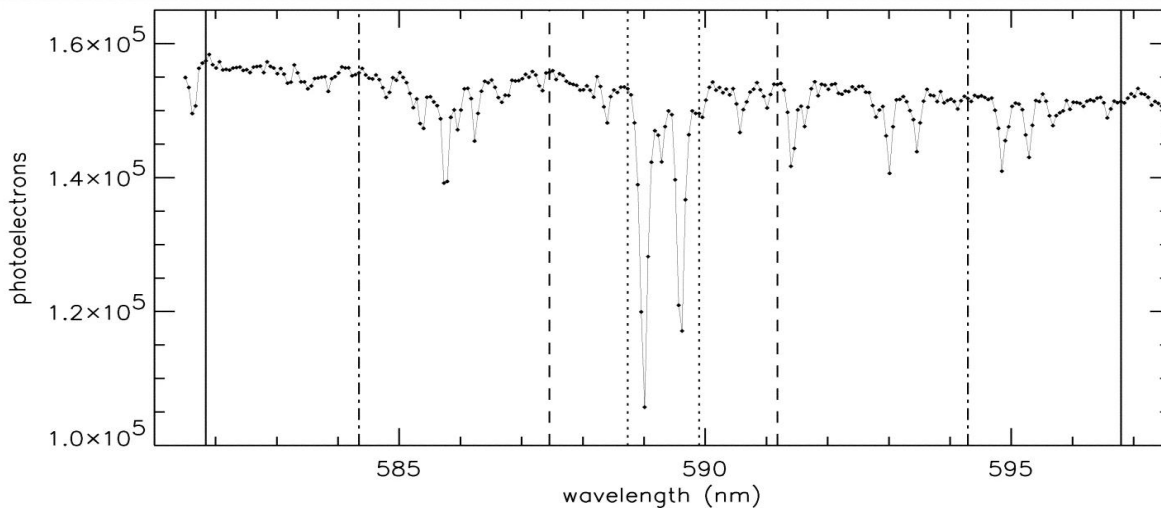

Figure 1. A portion of the spectrum of HD 209458b, obtained using HST/STIS and centered on the Na D lines (taken from Charbonneau et al. 2002).

Infrared spectroscopy is the most powerful tool we have to obtain information about the composition and temperature of exoplanet atmospheres. Models have been used since 1998 to predict the composition of the atmospheres of bright, transiting hot-Jovian exoplanets[3,4]. In 2002, Charbonneau et al. published the results of their analysis of spectra from transits of HD 209458; this was the first successful result to be published[5]. The observed spectrum, Figure 1, confirmed the predictions and, for the first time, allowed reasonable constraints to be placed on the atmosphere. Until now, using a space-based instrument, like HST or Spitzer, was the only way to perform an analysis of this type. Recent advancements indicate that it is possible to perform infrared spectroscopy of exoplanets using ground-based facilities.

Using the IRTF/SpeX combination, Swain et al. recently became the first to successfully obtain a dayside spectrum of HD 189733b from the ground[6]. The conclusion from these eclipse data is that ground-based spectroscopy can reproduce space-based measurements, and that new and unexpected information can be gathered using ground-based telescopes. While calibrating and analyzing data collected from a ground-based facility comes with its own set of challenges, Swain et al. developed a novel calibration method to deal with them. Figure 2 is a comparison of the results obtained from IRTF/SpeX, HST, and Spitzer[6]. The results of this method reveal a CO_2 absorption feature between 2.0 and 2.4 µm, which is in good agreement with previous HST measurements. Between 3.1 and 4.1 µm, the data agreed with Spitzer measurements within 1-σ[6,8]. The IRTF/SpeX data in this range show an emission feature that is much stronger than is typical for the other wavelengths in the spectrum. Currently, there are no space-based instruments that would be able to detect this feature at this spectral resolution. This gives us the opportunity to draw even more conclusions about the structure of the atmosphere of HD 189733b than would be possible with space-based measurements alone.
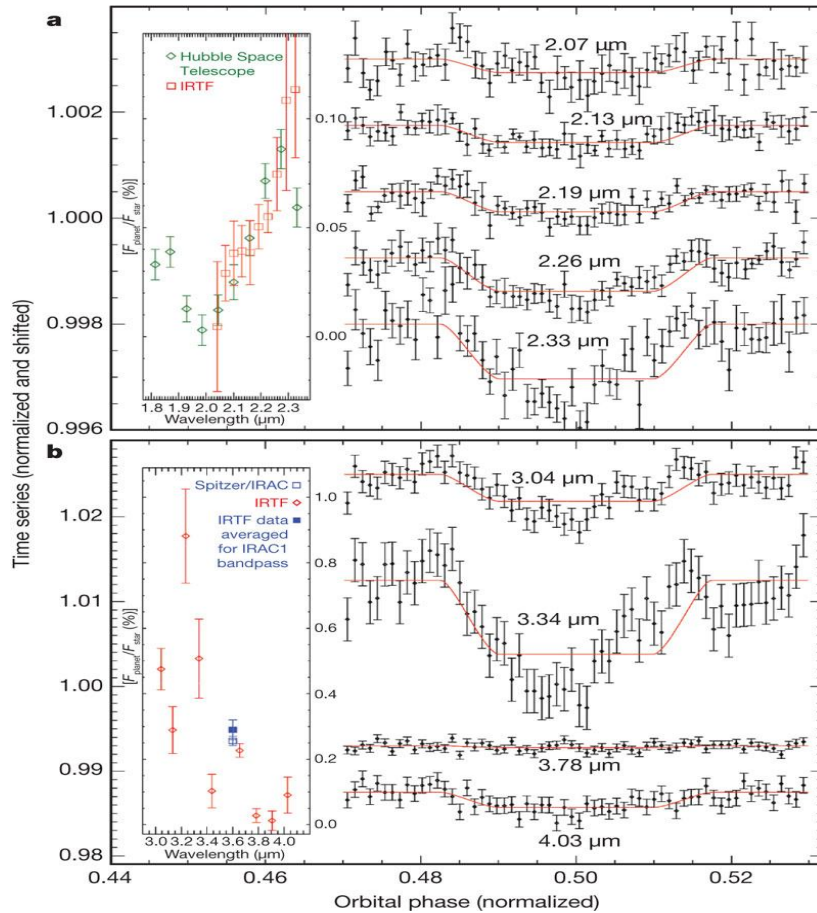

Figure 2. *Top Inset:* A comparison of the IRTF measurements with previous HST measurements. *Bottom Inset:* A comparison of the IRTF spectrum and the IRTF data averaged to the Spitzer 3.6µm pass band (solid square) with the Spitzer Space Telescope 3.6µm photometry measurement (open square). At right in both top and bottom are the calibrated light curve data (solid diamonds) and best fit eclipse model (solid line).

The results of Swain et al. open the door for small, ground-based observatories, to make giant strides in the study of exoplanets. This will require new instruments to be developed that are prepared to handle the challenge. One such observational tool is the New Mexico Tech Extrasolar Spectroscopic Survey Instrument (NESSI) which will exploit the calibration method developed by Swain, M.D., 2010. NESSI is being designed and built using funds allocated from the Magdalena Ridge Observatory, as well as a NASA EPSCoR grant awarded to scientists at New Mexico Tech. It will be a purpose built near-infrared spectrometer for operation on the Magdalena Ridge Observatory (MRO) 2.4 meter telescope[9].

2. TELESCOPE SPECIFICATIONS

The MRO 2.4m telescope is located on the South Baldy Ridge of the Magdalena Mountains, New Mexico, at an elevation of ~3200m. Its f/2.03 primary was one of three originally commissioned for the Hubble Space Telescope, and was donated to MRO. The primary science mission for the telescope is to observe, track, and characterize solar system astronomical targets, satellites, and space vehicles. The telescope, manufactured by EOS Technologies, is capable of slew rates up to 10°/sec, and accelerations of $3°/s^2$, which allow it to be used to observe objects in low-Earth orbit. Table 1 lists the relevant telescope specifications.

Table 1. Telescope specifications for the MRO 2.4m.

Telescope Specifications	
Manufacturer	EOS Technologies, Inc. of Tucson, AZ
Optical Design	Modified Ritchey-Chretien
Telescope Mount	Altitude – Azimuth
Surfaces	3 (Hyperbolic primary/secondary, flat tertiary)
Entrance Pupil Diameter	2.4m
Effective Focal Length	21.251m
Working f/#	8.856
Field of View	15 arcminutes
Image Scale	9.706 arcseconds/mm
Open-loop Tracking	0.5" in 5 minutes (specification)
Closed-loop Tracking	0.2" over 1 hour (specification)
6 Instrument Ports	2 Nasmyth/4 bent Cassegrain

3. NESSI DESIGN REQUIREMENTS

NESSI was conceived as the idea for an instrument that could accomplish, from the ground, what has only been accomplished previously with other spectrometers prior to 2009 using space-based platforms. NESSI is being designed to accomplish the goal of taking moderate resolution spectra in the infrared, where molecular constituents are abundant, in such a way as to be highly calibratable and repeatable. In order to be successful at this, NESSI must have four design goals:

1. Instrument must quickly assess spectra of transiting exoplanets during transits, and in the presence of the parent star's (much larger) flux.
2. Instrument must be stable over short (tracking) and long (repeat visit) timescales.
3. Must have simultaneous coverage of both target and calibrators (multi-object capabilities).
4. Must be on a dedicated platform that can be readily accessed so that transits can be measured whenever they happen, and readily as new missions indentify new targets.

Table 2. NESSI instrument design requirements.

Measurable	Design Goal
Telescope Focal Station	Nasmyth
Operational Wavelengths	1.1 to 2.4μm (J/H/K)
Modes of Operation	Low – Res (R~250) across J, H, & K; Moderate – Res (R~1000) in each band; Imaging
Field of View	Infrared: 12 arcminutes; Optical: 4 arcminutes
Pixel Scale	Infrared: 0.5 arcsecond/pixel
Direct Imaging	Over entire FOV
Image Quality	EE80 ≤ 1 pixel = 1 arcsec = 36μm
Guiding	Optical at 1-5Hz rate and 0.3 arcsecond accuracy
System Throughput	20% minimum
Stability of Image at Mask	Due to drifts (derotator or telescope) 0.3 arcseconds
Multi-object Apertures	3 to 5 arcseconds, with MOS separations of 6.0 arcseconds in the spatial direction
Masks in Wheel	Minimum of 8 exoplanet fields plus open and dark
Dewar Hold Time	Minimum 36 hours

4. OPTICAL DESIGN

The underlying design philosophy for NESSI is simplicity. It is driven by the need to get the instrument on the sky in as short a time as possible to maximize the scientific product. To accomplish this, the optical design is one that: 1) keeps the number of moving parts to a minimum, 2) has all spherical powered optics, 3) uses commonly available materials, and 4) minimizes surface diameters as much as possible. The design also emphasizes modularity, which allows for the different units to be designed and constructed independently from one another. Figure 3 presents a ray trace of the telescope – NESSI optical train. NESSI can be divided into four distinct units:

1. <u>Field Derotator</u>: Functions to remove field rotation at the Nasmyth port. It consists of a field lens and a k-mirror.

2. <u>Reimager</u>: Reimages the telescope focal plane on the spectrograph multi-object mask. It consists of a pair of doublets, a dichroic to split the visible (guiding) and IR (science) channels, and the dewar window/field lens.

3. <u>Autoguider</u>: Stabilizes telescope tracking errors by feeding back pointing corrections directly to the mount. It operates in the visible, and consists of imaging optics and a detector.

4. <u>Spectrograph</u>: Selects the target and calibrator objects in the field, spectrally disperses the light, and senses the dispersed spots. It consists of a multi-object mask, collimator and camera group of optics, spectral filters, dispersing elements, and a detector.

As indicated in Table 2, and in the above breakdown of the four units, NESSI will have two channels of operation: 1) an IR (J/H/K) channel for science observations, and 2) a visible channel for autoguiding where corrections in tracking are fed back directly to the telescope mount. There are three focus locations inside of the instrument; the first is inside the derotator and is controlled by the telescope; the second is at the multi-object mask inside the spectrograph and is controlled by adjusting the reimaging optics, and the third is at the detector.
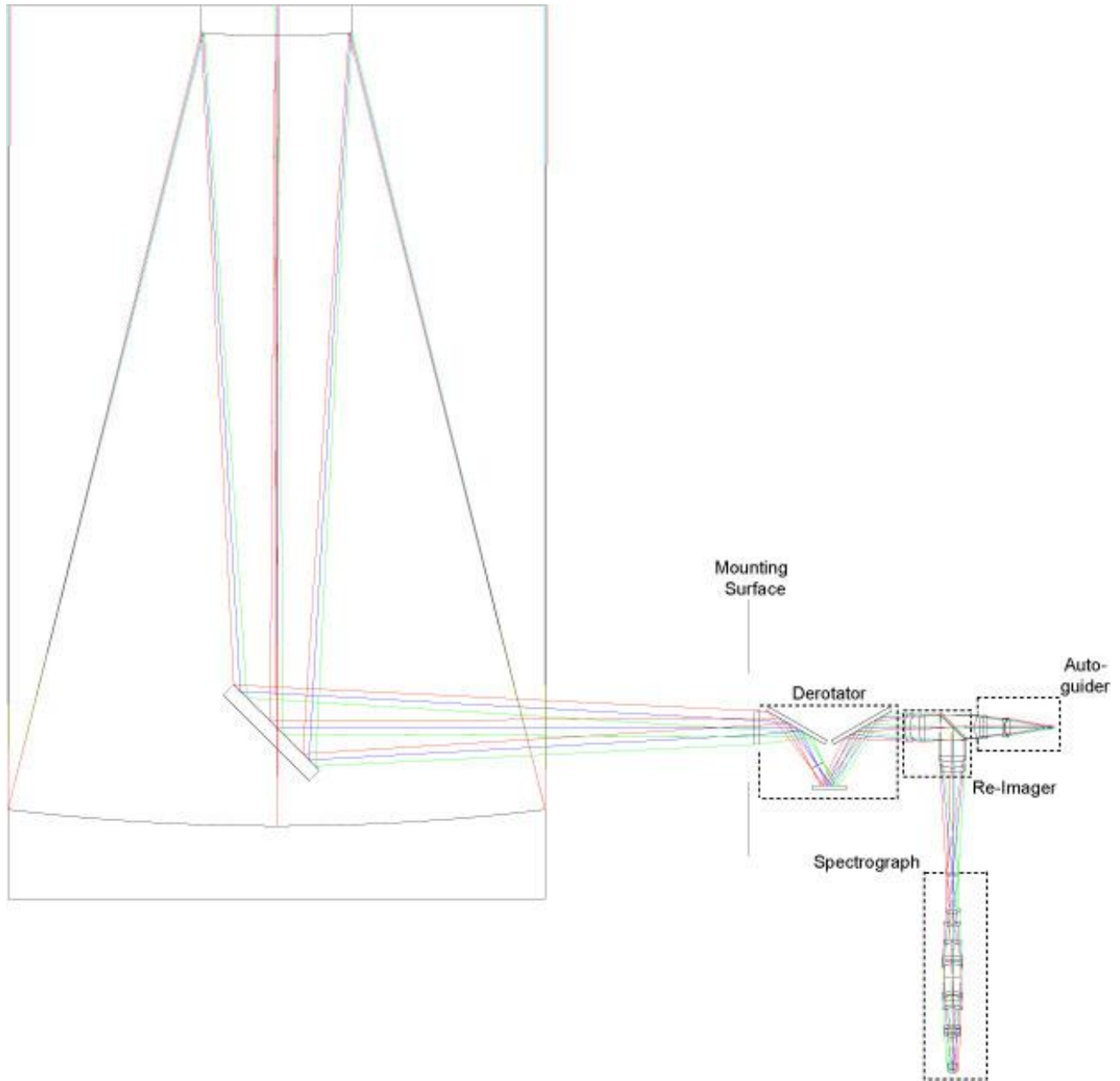
Figure 3. Ray trace of the 2.4m – NESSI optical train. The location of the telescope mounting surface in relation to NESSI's four optomechanical modules are labeled.

4.1 IR Glass Selection

The optical design for the IR channel of NESSI was built up through combinations of doublets and triplets to achieve apochromatic correction at two locations within the instrument. The first of these is the multi-object mask following the dewar window, and the second is on the spectrograph detector. There are also two locations that provide an image of the pupil; one is at the dichroic that splits the IR and visible channels, and the other is the location of the Lyot stop within the dewar.

Ren & Allington-Smith[10] investigated the use of the Herzberger relative-partial-dispersion – V-number equation at near-IR wavelengths[11] as an approach to optimizing glass combinations for doublets and triplets. The results of the

investigation enable the selection of doublet and triplet materials directly from the partial dispersion – V-number plot. Figure 4 plots this for some commonly chosen materials in IR applications. The stars in the figure are the locations of the materials chosen for the NESSI doublet/triplet combinations.

In selecting suitable doublet materials for three color correction, the above investigators determined that the slope of the line connecting the points between the two materials is proportional to the amount of secondary residual chromatic aberration. The amount of power that must be introduced by these elements to correct for this is inversely proportional to the length of the line separating the two materials. It is therefore ideal to have two materials with similar partial dispersion, but a large difference in V-number. External to the cryostat, the doublet combinations chosen were CaF_2/Infrasil, and the internal combinations are BaF_2/Infrasil.
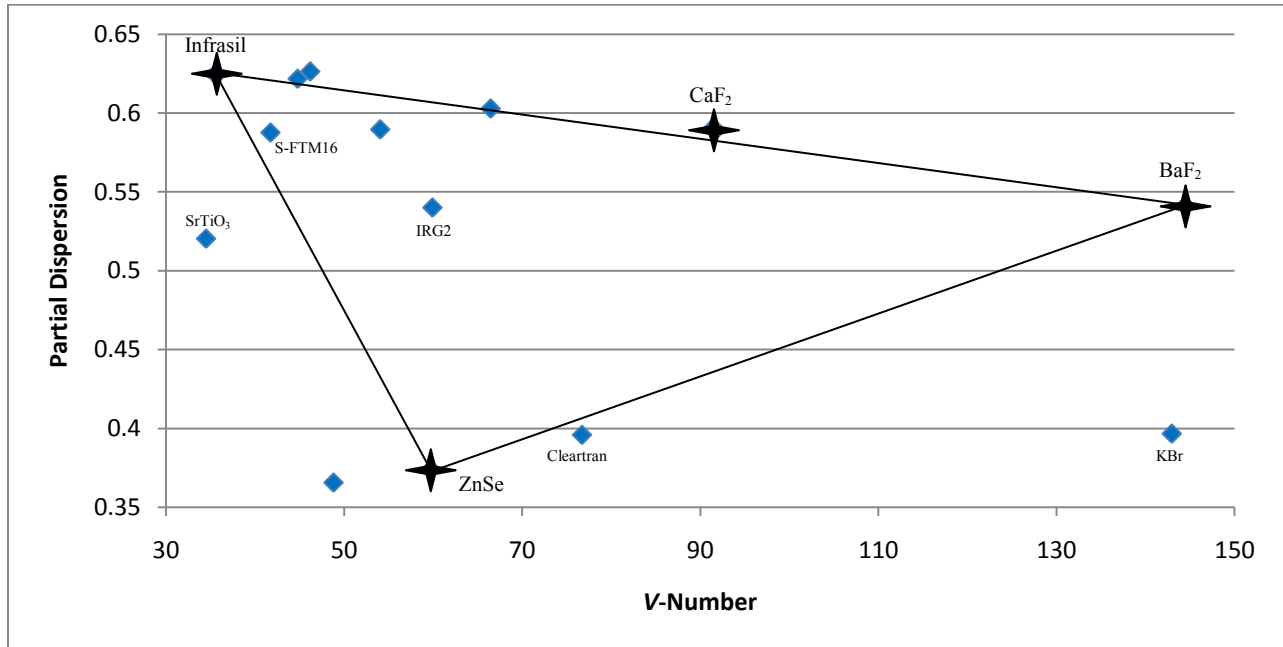

Figure 4. Partial dispersion versus V-number for a sample of IR materials. The diamonds are common materials in IR applications. The four stars mark the locations of Infrasil, ZnSe, CaF_2, and BaF_2, the materials chosen for doublet/triplet combinations in NESSI.

Triplets are only used inside of the cryostat, and consist of Infrasil/BaF_2/ZnSe. The objective in selecting triplet materials is to reduce the higher order aberrations by minimizing the optical powers of the three elements. Without going into the details of the paper, the conclusion was that the power of the three elements will be minimized when the chosen materials maximize the area of a triangle bounded by the three lines that connect them on the P – V plot. This is marked by the three lines in the figure above for the NESSI materials.

4.2 NESSI System Layout

Figure 5 is the NESSI ray trace from the from the telescope output to the spectrograph detector. Distances are labeled from the Nasmyth mounting surface to the pivot point of the dichroic, from the dichroic to the dewar window, and from the dewar window to the detector. The total field of view is 12 arcminutes, with wavelengths ranging from 1.1 to 2.4μm. The three focii (inside derotator/spectrograph mask/detector) are clearly visible as well as the two pupil images (dichroic/inside spectrograph). Rays to the autoguiding unit have been omitted as this portion of the instrument is not of interest for this paper.
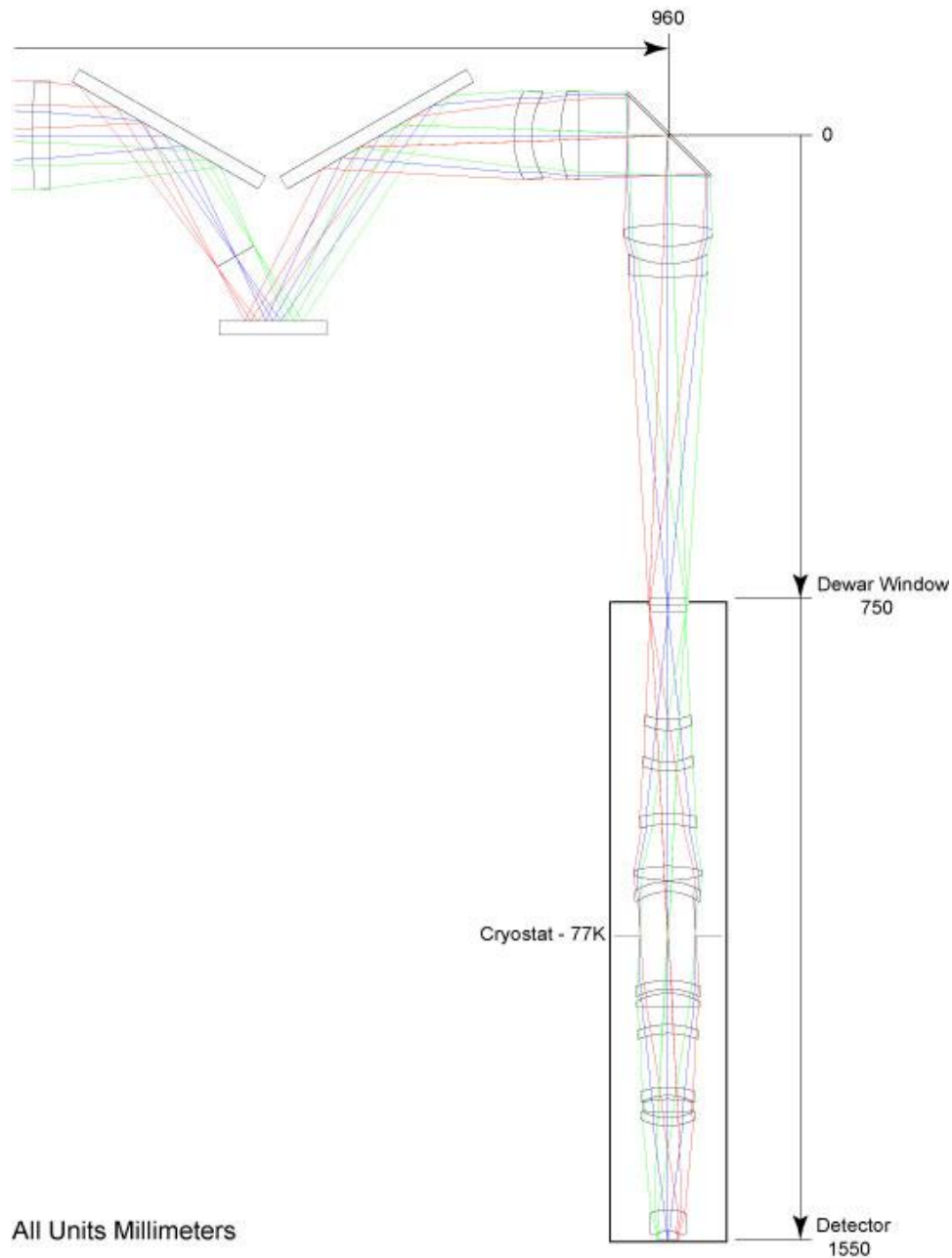
Figure 5. NESSI optical train and dimensions excluding the autoguider unit. All units are in millimeters and dimensions are relative to the dichroic. The telescope mounting surface is at the upper left.

4.3 Mask Reimaging

Figure 6 is a close-up view of the optics from the telescope output to the spectrograph mask. FL-1 converts the f/8.856 telescope output to an f/5.837. The beam is then collimated by the first Infrasil/CaF$_2$ doublet (REI-1/2), and the IR light gets reflected by the dichroic. A second, CaF2/Infrasil doublet (REI-3/4), reimages the telescope focal plane at f/4.722 upon the multi-object mask. The second field lens, FL-2, in addition to relaying the magnified field, also serves as an additional variable in the optimization to match the exit pupil position and diameter of these reimaging optics to the spectrograph entrance pupil.
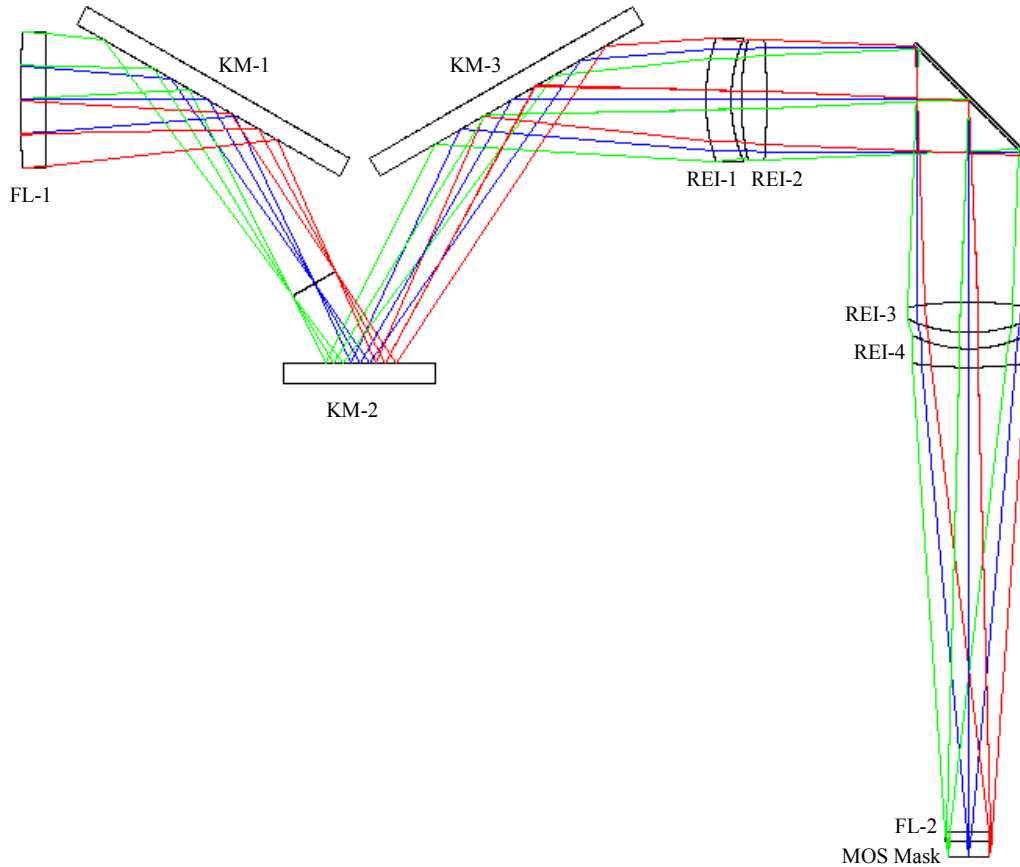
Figure 6. Ray trace from telescope output through reimaging optics to the spectrograph mask. Table 3 lists the materials and sizes associated with each of the elements.

Table 3. Element specifications for Figure 6.

Element	Clear Aperture (mm)	Material
FL-1	140	Cleartran
KM-1/KM-2/KM-3	<150	Mirrors
REI-1	120	Infrasil
REI-2	120	CaF_2
REI-3	120	CaF_2
REI-4	115	Infrasil
FL-2	50	ZnSe

It was stated previously that the 'multi-object' selection will be done with masks that have aperture diameters of 3 to 5 arcseconds for the targets and calibrators. It has yet to be determined what the optimal diameter is, but should be pointed out that the primary reason for the apertures is the removal of background and other stray light that may enter the system. Figure 7 is the encircled energy plot at the mask for all fields and wavelengths. From this plot, it is shown that the ideal performance taking into account all optics in the train from telescope to mask yields >80% EED at 3", and that essentially all the light gets through at 5". The bold lines mark the location of the radii for 3 and 5 arcseconds.
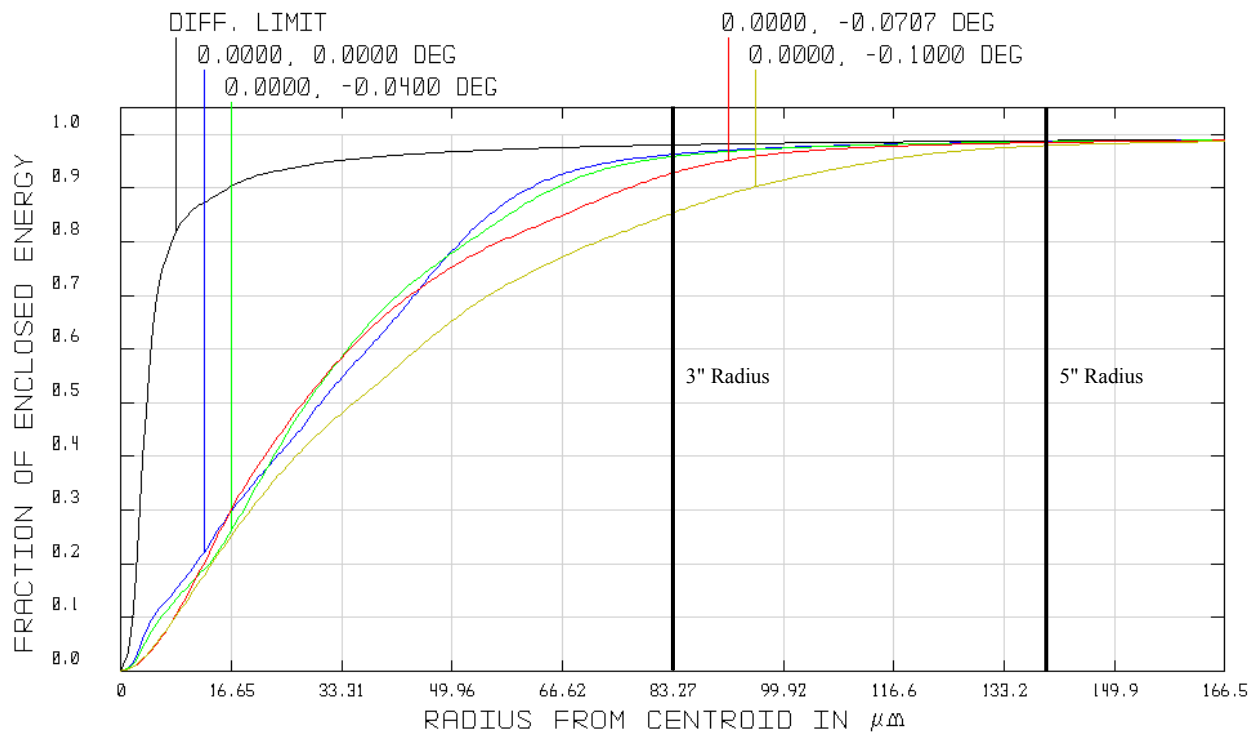
Figure 7. EED for all fields and wavelengths at the multi-object mask. The bold lines mark the radii for 3 and 5 arcseconds. This plot takes into account all optics from telescope to mask.

4.4 Spectrograph

The spectrograph is comprised of two groups of powered optics: a collimator group, and a camera group. The collimator group consists of 5 lenses (doublet/triplet combination), and serves to capture the fairly large field of view (12' on sky/8° at the mask) and produce an image of the pupil for a Lyot stop. The filter/GRISM combinations (not shown above – discussed in Section 4.5) will straddle the Lyot stop. Figure 8 is the spectrograph ray trace.
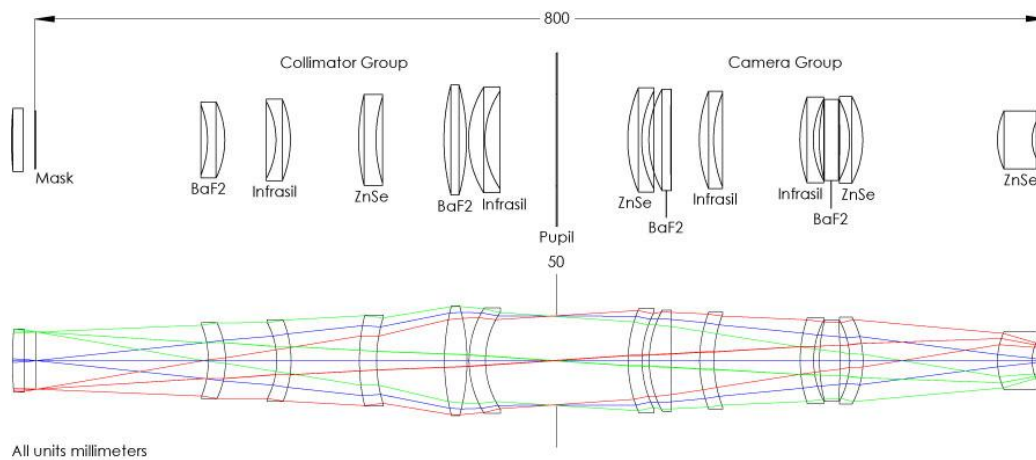

Figure 8. The spectrograph consists of two powered groups of optic following the mask: a collimator group and the camera group. The total track length is 800mm, and the pupil diameter is 50mm.

The camera group consists of 7-elements (two triplets and a field flattener). The collimator has an angular magnification of 1.2 which results in a 4.8° half field for the camera. It reimages the mask at f/3 onto the detector, giving a plate scale of 0.5 arcseconds per pixel. Figure 9 is polychromatic ensquared energies at the detector for all fields. The bold lines indicates the Hawaii pixel half-width. Each pixel has >80% ensquared energy for the telescope – NESSI system, with essentially all the light falling within a 3x3 pixel box.
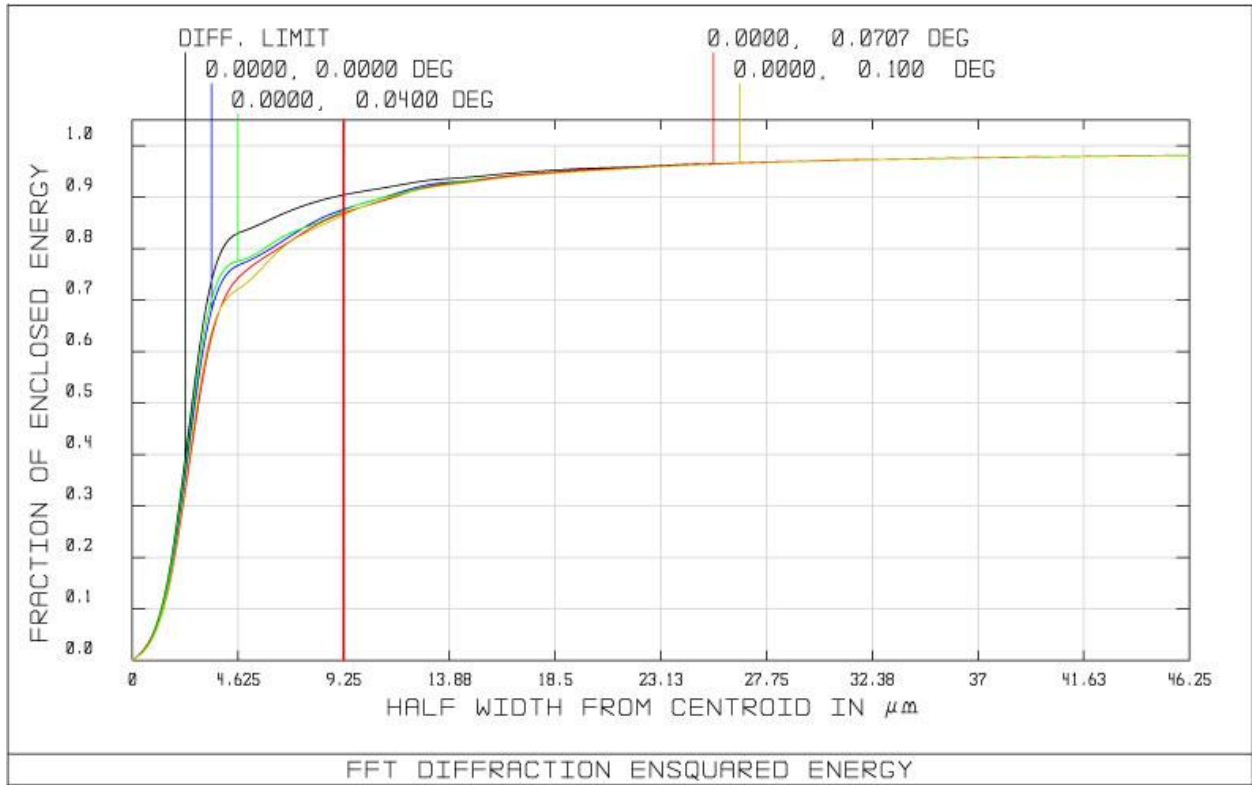

Figure 9. Polychromatic diffraction ensquared energy at the detector. Requirement is >80% at 0.5" per pixel.

4.5 GRISMs

In this section the optical design chosen for carrying out the dispersion is presented. There are two resolution modes that will be offered by NESSI; a low resolution mode with R ~ 250 across the entire J, H, K region, and a high resolution mode with R ~ 1000 within each of the bands. The GRISMs have been designed to operate in 'direct view,' and will be manufactured by Newport RGL, using reflectance gratings from their standard catalog as templates for the transmission gratings.

4.5.1 Grating Selection

This section will briefly outline the process by which the gratings were chosen, for a more detailed discussion on GRISM design, see Traub[12]. The number of spectral channels, N_c, is related to the spectral dispersion by:

$$N_c = R \times \frac{\Delta\lambda}{\bar{\lambda}}$$

where $\Delta\lambda$ is the spectral bandwidth and $\bar{\lambda}$ is the mean wavelength. The linear dispersion, ΔX, of the grating can then be related to the groove density of the grating σ and the focal length of the spectrograph f by:

$$\Delta X = \frac{m\sigma f}{\cos(\beta)}\Delta\lambda$$

where m and β are the working order (m = 1 in this case) and the angle of diffraction respectively. The number of spectral channels N_c is also related to the linear dispersion by:

$$\Delta X = 2 \times N_c \times p$$

where p is the pixel size of the camera. The factor of two in the last equation is ensure that we are Nyquist sampling the seeing. For a given desired resolution, the ideal groove density, σ, can then be calculated. It is ideal because Newport doesn't necessarily have that exact groove density in their catalog. So in each case, the closest to ideal was chosen. There is one final consideration when choosing the appropriate catalog reflection grating to be used in transmission from Newport. The blaze wavelength of the grating, i.e. the peak efficiency wavelength, is significantly different when the grating is used in reflection or in transmission. The rule of thumb relation between the blaze wavelength of the reflection grating $\lambda_{b,r}$ and the blaze wavelength of the transmission $\lambda_{b,t}$ grating is:

$$\lambda_{b,r} = \frac{2}{n_g - 1}\lambda_{b,t}$$

where n_g is the grating index of refraction. Newport RGL uses epoxies with $n_g \sim 1.52$, thus we have to look for reflection gratings in the Newport catalog with:

$$\lambda_{b,r} = 3.8\lambda_{b,t}$$

The next two sections will reveal the grating selection for each resolution mode (one low-res/three moderate-res), and the resulting resolutions.

4.5.2 Low Resolution Mode

The low resolution mode has a goal of R = 250 for the entire spectral band JHK = [1.17 to 2.37]µm. From the above equations, the optimal groove density of the grating is σ_{JHK} = 23 lines/mm. Table 4 lists the closest to optimal grating that was found in the Newport catalog. In order to obtain the maximum efficiency for the GRISMs, the prism apex angle has to be equal or as close as possible to the blaze angle. Moreover, the index of refraction of the prism impacts the diffraction angle through the GRISM. Thus, it is necessary to choose a prism material that will yield an apex angle close to the blaze angle when in direct-view. The resulting resolution for the low resolution mode is R = 214.

Table 4. GRISM specifications for the low resolution mode.

	Selected Reflection Grating	Reflection Blaze Wavelength	Theoretical Transmission Blaze Wavelength	Groove Density (lines/mm)	Blaze Angle	Prism Angle	Prism Material
JHK	53-*-933R	8.0µm	2.1µm	30	6.9°	6.9°	Infrasil

4.5.3 High Resolution Mode

The high resolution has a goal of R = 1000 within each of the bands. J [1.17 to 1.33], H [1.49 to 1.78], and K [2.03 to 2.37]. Table 5 lists the standard gratings that were chosen from Newport, and the resulting GRISM specifications. As with the low resolution mode, the prism material was chosen to match the prism and blaze angles as closely as possible while maintaining the direct view condition. The resulting resolutions for the three bands are: R_J = 998, R_H = 1113, and R_K = 1048.

Table 5. GRISM specifications for the moderate resolution modes.

	Selected Reflection Grating	Reflection Blaze Wavelength	Theoretical Transmission Blaze Wavelength	Groove Density (lines/mm)	Blaze Angle	Prism Angle	Prism Material
J	53-*-870R	4.5μm	1.2μm	180	23.9°	23.1°	S-FTM16
H	53-*-880R	6.0μm	1.6μm	150	26.7°	25.6°	S-FTM16
K	53-*-876R	8.6μm	2.3μm	105	26.7°	24.4°	S-FTM16

4.6 System Throughput

Table 6 is the system throughput calculation for the NESSI optical train only for each of the resolution modes. The worst case was found to be for the J-Band, with a total throughput of 28%. The design requirement from Table 2 was 20%, so this should easily be met.

Table 6. System throughput for the NESSI optical train for each of the resolution modes. Worst case is found to be that for J-Band at 28%. This meets the overall system requirement of 20%.

		Number of reflections or transmission	J band transmission	H band transmission	K band transmission	JHK band transmission		
			AR Coating VIS+IR					
Coating Transmission			0.992	0.994	0.997	0.992	0.994	0.997
Derotator	Field lens	2	0.984	0.988	0.994	0.984	0.988	0.994
	K-Mirror	3	0.941 (0.98^3)					
Sub-total			0.926	0.930	0.935	0.926	0.930	0.935
Reimager	2 Lenses	4	0.968	0.976	0.988	0.968	0.976	0.988
			AR Coating IR					
Coating Transmission			0.994	0.994	0.996	0.994	0.994	0.996
	2 Lenses	4	0.976	0.976	0.984	0.976	0.976	0.984
	Mask		0.95					
	Field lens	2	0.988	0.988	0.992	0.988	0.988	0.992
Sub-total			0.887	0.894	0.916	0.887	0.894	0.916
Spectrograph (w/o the grisms)	12 Lenses	24	0.865	0.865	0.908	0.865	0.865	0.908
Grisms	2 Surfaces		0.96 (0.98^2)					
	Grating >		0.55	0.80	0.70	0.45	0.65	0.80
Sub-total			0.343	0.664	0.610	0.374	0.540	0.697
Quantum efficiency			0.80					
TOTAL			0.281	0.552	0.522	0.307	0.450	0.597

ACKNOWLEDGEMENTS

REFERENCES

[1] Wolszczan, A.F., Frail, D.A., "A Planetary System Around the Millisecond Pulsar PSR1257+12," Nature, 355, 145 (1992).

[2] Schneider, J., "Interactive Extra-solar Planets Catalog Version 2.02," http://exoplanet.eu/catalog-all.php

[3] Seager, S.S., Sasselov, D.D., "Extrasolar Planets Under Strong Stellar Irradiation," ApJ, 502, L157 (1998).

[4] Seager, S.S., Sasselov, D.D., "Theoretical Transmission Spectra During Extrasolar Giant Planet Transits," ApJ, 537, 916 (2000).

[5] Charbonneau, D.B., Brown, T.M., Noyes, R.W., Gilliland, R.L., "Detection of an Extrasolar Planet Atmosphere," ApJ, 568, 377 (2002).

[6] Swain, M.R., Deroo, P., Griffith, C.A., Tinetti, G., Thatte, A., Vasisht, G., Chen, P., Bouwman, J., Crossfield, I.J., Angerhausen, D., Afonso, C., Henning, T., "A Ground-Based Near-Infrared Emission Spectrum of the Exoplanet HD 189733b," Nature, 463, 637 (2010).

[7] Swain, M.R., Vasisht, G., Tinetti, G., "The Presence of Methane in the Atmosphere of an Extrasolar Planet," Nature, 452, 329 (2008).

[8] Charbonneau, D.K., Knutson, H.A., Barman, T., Allen, L.E., Mayor, M., Megeath, S.T., Queloz, D., Udry, S., "The Broadband Infrared Emission of the Exoplanet HD 189733b," ApJ, 686, 1341 (2008).

[9] Ryan, E.V., Ryan, W.H., "The Magdalena Ridge Observatory's 2.4-meter Telescope: A New Facility for Follow-up and Characterization of Near-Earth Objects," Proceedings of the 2008 AMOS Technical Conference, 402-408.

[10] Ren, D., Allington-Smith, J.R., "Apochromatic Lenses for Near-Infrared Astronomical Instruments," Opt. Eng., 38, 537 (1999).

[11] Herzberger, M., Salzberg, C.D., "Refractive Indices of Infrared Optical Material and Color Correction of Infrared Lenses," JOSA, 52, 420 (1962).

[12] Traub, W.A., "Constant-dispersion GRISM Spectrometer for Channeled Spectra," JOSA, A7, 1779-1791 (1990).